Journal of Sound and Vibration (2002) **250**(2), 229–245
doi:10.1006/jsvi.2001.3920, available online at http://www.idealibrary.com on IDEAL®

CHAOS AND MULTIPLE PERIODS IN AN UNSYMMETRICAL SPRING AND DAMPING SYSTEM WITH CLEARANCE

MD. Z. HOSSAIN, K. MIZUTANI AND H. SAWAI

Department of Mechanical Engineering, Faculty of Engineering, Mie University, 1515 *Kamihama-cho, Tsu, Mie* 514-8507, *Japan. E-mails: zahid@ss.mach.mie-u.ac.jp; mizutani@ss.mach.mie-u.ac.jp; sawai@ss.mach.mie-u.ac.jp*

(*Received* 24 *October* 2000, *and in final form* 1 *May* 2001)

Chaos and multiple periods are presented for the harmonically excited unsymmetrical spring and damping system with clearance. This paper demonstrates the non-linear behaviour of the motion through simulation and experiment. Intensive care and caution are taken in the experiments to observe the chaos and the multiple periods properly. The focus in this paper is mainly on the change of the bilinear spring stiffness ratio as a prime factor by which chaotic motions occur from quasi-periodic motion. Other investigations and effects on motion are also discussed for the changing of the extent of clearance. The investigations are based on frequency response curves. To understand the dynamics of the non-linearity of this model, all possible data processing and displaying techniques are taken into account. To observe the overall phenomena of this bilinear system, the resonance curves and the bifurcation diagrams are taken thoroughly for a wide frequency region.

1. INTRODUCTION

A system for the changing of the abrupt stiffness and damping factor is defined as a piecewise linear system in the non-linear dynamics. The piecewise linear system has a practical interest in many mechanical systems such as supports with motion limiting stops, mechanical systems having clearances or snubbers. A theoretical demonstration of the piecewise linear system has been found in many papers [1–17] and, an experimental demonstration has been found in a few papers [3, 17].

Clearance exists in many practical systems: clearance in coupling of rotor-coupling system, clearance in bearing of shaft-bearing system, backlash in gear rattling, clutch-power transmission system, etc. As clearance makes a system strongly non-linear, the system can exhibit chaotic, super-harmonic and sub-harmonic responses. Non-periodic motion has been established in the stability analysis literatures [2, 13, 14]. The damping factor has also great effect in causing the non-periodic motions on the non-linear system [15]. The clearance problem has been modelled as a single degree of freedom from early literatures [2, 4, 5, 7] to recent ones [3, 15, 17, 18]. Multi-degree-of-freedom model has been carried out recently in some literatures [11, 12]. The focus in the above literatures is mostly concentrated on symmetrical model for the clearance problem. Our previous study [3] has demonstrated the frictional effect mainly on both of the symmetric and asymmetric models.

Chaos, a random-like non-periodic motion, has been a subject of interest for many years [6, 7, 16–26]. There are different routes to chaos. Period-doubling route to chaos is the most

0022-460X/02/070229 + 17 $35.00/0

frequently observable route to chaos in the non-linear dynamics, which are depicted in some literatures [6, 16, 25]. The Feigenbaum number is popular to distinguish this type of route to chaos. The second type of route to chaos, intermittent route to chaos, is demonstrated in literature [7]. The intermittency occurs due to the sudden changes of the size of chaotic attractors, sudden appearances of the chaotic attractors (a possible route to chaos), and sudden destructions of the chaotic attractors and their basin [21, 22]. Quasi-periodic route to chaos is the third type of route to chaos [19].

An extensive discussion is available in literature [7] for the bilinear stiffness system free in the clearance, and also elastically connected in the clearance. The intermittent route to chaos has been observed mostly in this literature. Experimentally, Wiercigroch *et al.* [17] have shown through bifurcation diagram in some specific frequency regions that symmetrical bilinear system with clearance can show the chaos. The conclusion of this literature is that the chaotic motion occurs more in the symmetrical bilinear system, as the ratio of the extent of clearance to the harmonic excitation amplitude is decreased.

In our study, the model is considered as an unsymmetrical bilinear and a one-degree-of-freedom model with clearance. The unsymmetrical bilinear system with clearance has not been investigated properly through simulation and experiment. This study thoroughly demonstrates the performance of the system for a wide range of frequency regions instead of some specific frequency regions. The comparison and the cause of the differences between simulations and experiments are also discussed through bifurcation diagrams and all other data processing and displaying techniques such as FFT, phase plane diagrams and Poincaré maps, etc.

The main purpose of this study is to investigate the chaotic phenomena and the multiple periods of a periodically excited unsymmetrical bilinear spring and damping system by the changing of the spring ratio and the clearance to the excitation amplitude ratio through experiments and simulations. An attempt was made to adjust the experimental set-up with the bilinear clearance model.

2. PHYSICAL AND CHARACTERISTIC MODEL

Figures 1(a) and 1(b) show the physical and the characteristic models of a bilinear spring and damping system with clearance. Clearance is visible in many types of rotary machinery. Coupling clearance is undertaken in this study. Coupling could be free or connected by some elastic material in the clearance of a rotor-coupling system or a power transmission-clutch system. A term, balance point is introduced to denote the starting point of vibration of the system from rest. The unsymmetrical bilinear system is modelled in this study where the position of the balance point is very near from the contact point and is held on the spring k_2 as in Figure 1(b). The reasonability of the unsymmetrical concept is that the bilinear system, especially having some preloaded conditions, could be hard to be symmetric, while the coupling is free or connected by a very low stiffness spring in the clearance. The characteristic models of the system free in the clearance and connected by spring in the clearance are shown in Figure 1(b). The extent of clearance is denoted by $(d_2 - d_1)$. The vibration starts from the balance point with the spring stiffness k_2. When the displacement of the vibration reaches within d_1 to d_2, the stiffness is changed to k_1. Then, again the stiffness is changed to k_2 when the displacement of the vibration exceeds d_2. The solid line denotes the zero stiffness slope of the spring k_1, whereas the dotted lines denote the higher stiffness slope of the spring k_1 than that of the solid line.

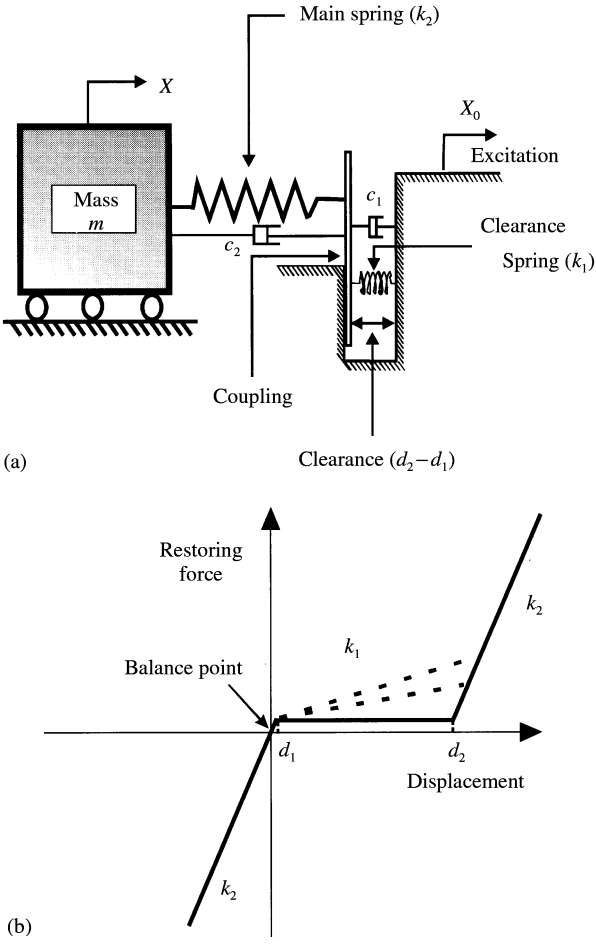

Figure 1. (a) Physical model. (b) Spring characteristic model.

3. ANALYTICAL MODEL

The three force conditions in unsymmetrical models with clearance (Figures 1(a) and 1(b)) are

$$f(X) = \begin{cases} k_2(X - X_0) + c_2(\dot{X} - \dot{X}_0), & X < d_1, \\ k_1(X - X_0 - d_1) + k_2 d_1 + c_1(\dot{X} - \dot{X}_0), & d_1 \leqslant X \leqslant d_2, \\ k_2(X - X_0 - d_2 + d_1) + k_1(d_2 - d_1) + c_2(\dot{X} - \dot{X}_0), & X > d_2. \end{cases} \quad (1)$$

The excitation displacement X_0 being taken as $E\sin(\omega t)$, the equations of motion become

$$\begin{aligned} &m\ddot{X} + c_2\dot{X} + k_2X = k_2E\sin(\omega t) + c_2E\omega\cos(\omega t), && X < d_1, \\ &m\ddot{X} + c_1\dot{X} + k_1X = k_1E\sin(\omega t) + c_1E\omega\cos(\omega t) - (k_2 - k_1)d_1, && d_1 \leqslant X \leqslant d_2, \\ &m\ddot{X} + c_2\dot{X} + k_2X = k_2E\sin(\omega t) + c_2E\omega\cos(\omega t) + (k_2 - k_1)(d_2 - d_1), && X > d_2. \end{aligned} \quad (2)$$

The equations can be rewritten in the non-dimensional form as

$$\begin{aligned} &\ddot{x} + \xi_2\dot{x} + x = \sin(\Omega\tau) + \xi_2\Omega\cos(\Omega\tau), && x < \delta_1,\\ &\ddot{x} + \xi_1\dot{x} + \alpha x = \alpha\sin(\Omega\tau) + \xi_1\Omega\cos(\Omega\tau) - (1-\alpha)\delta_1, && \delta_1 \leqslant x \leqslant \delta_2,\\ &\ddot{x} + \xi_2\dot{x} + x = \sin(\Omega\tau) + \xi_2\Omega\cos(\Omega\tau) + (1-\alpha)2\beta, && x > \delta_2, \end{aligned} \tag{3}$$

where $X/E = x$, $p_1^2 = k_1/m$, $p_2^2 = k_2/m$, $\tau = p_2 t$, $\delta_1 = d_1/E$, $\delta_2 = d_2/E$, $\Omega = \omega/p_2$, $\xi_1 = c_1/mp_2$, $\xi_2 = c_2/mp_2$, $\alpha = k_1/k_2$, $2\beta = (\delta_2 - \delta_1)$ and $(\cdot)$ represents the differentiation with respect to τ.

4. EXPERIMENTAL SET-UP

Figure 2 shows the experimental set-up. Harmonic excitation, $E\sin(\omega t)$, is imparted into the system by the motor-crank device. The eddy current sensors measure the excitation displacement (X_0) and the displacement (X) of the mass m. The eddy current sensor (X_1) measures the clearance spring displacement. A fibre-optic sensor is shown as a timing signal for poducing a pulse per cycle of the excitation frequency. A voice coil actuator (Figure 2) is used as a coupling. A required force is applied into the system by the voice coil actuator for fixing the position of the system at the balance point. Figure 3 demonstrates the data processing and displaying techniques, and it is noted that no filter is used in data processing to avoid the change of phase of the signals. The parameters taken in the experiment are $m = 2{\cdot}1$ kg, $k_2 = 15$ N/mm, $E = 0{\cdot}225$ mm and the excitation frequency range $= 3{\cdot}6 \sim 36$ Hz.

5. NUMERICAL AND EXPERIMENTAL RESULTS

Figures 4–9 show the simulational and experimental results for the values of $\alpha = 0$, $0{\cdot}15$ and $0{\cdot}25$ while the value of the $\beta = 3$ in all of the three cases. A set of parameters, $\delta_1 = 0{\cdot}05$, $\xi_1 = 0{\cdot}01$ and $\xi_2 = 0{\cdot}05$ for the simulation, and $\delta_1 = (0{\cdot}04 \sim 0{\cdot}17)$ for the experiment, is kept constant in all of the three cases.

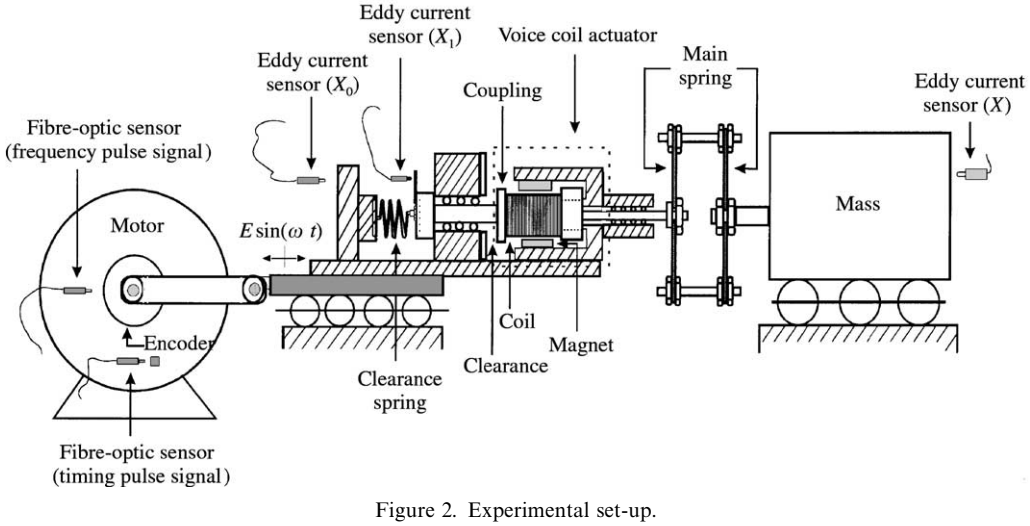

Figure 2. Experimental set-up.

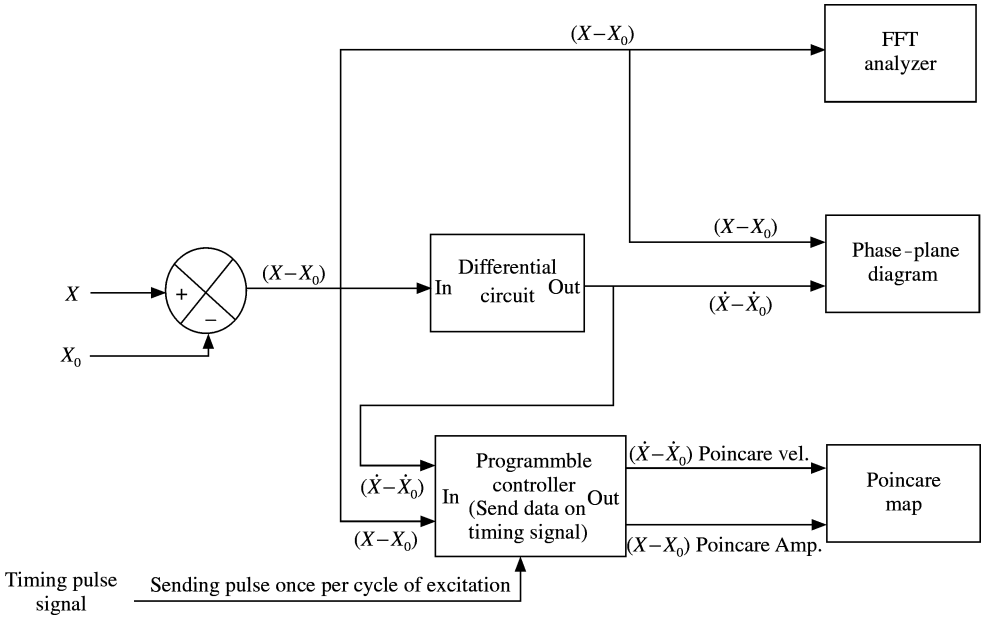

Figure 3. Data processing and displaying techniques.

Figure 4 shows the frequency response curves where the harmonic and the sub-harmonic resonances are observable. Bifurcation diagram (Figure 5) of the frequency response (Figure 4) demonstrates that the periodic, non-periodic and multiple periodic motion can occur with the gradual increase of the excitation frequency. In both simulation and experiment, it is shown that the non-periodic and the multiple periodic motions occur more by the decreasing of the value of α from 0.25 to 0. Periodic order is denoted by Pn. Chaos appears suddenly after P1 as an intermittent route to chaos. The periodic order is shown as P1 $\rightarrow$ Chaos $\rightarrow$ P3 $\rightarrow$ P5 for the spring ratio 0. The value of the spring ratio at $\alpha = 0{\cdot}15$ could be called as a transient spring ratio among the considered spring ratios where the non-periodic motion is approaching to diminish but other sub-harmonic resonances are observable. Chaos appears suddenly, and the response exhibits chaotic motion for a short-frequency region as a combination of the unstable periods of P2, P4, P6. Periodic order is shown as P1 $\rightarrow$ Chaos $\rightarrow$ P2 $\rightarrow$ P6 $\rightarrow$ P3 $\rightarrow$ P6 $\rightarrow$ P3 (Figure 5(b′)). Strong non-linearity is lagging at $\alpha = 0{\cdot}25$; the bifurcation diagram shows only the P1 and P2 (Figures 5(c) and 5(c′)). The multiple periods also disappear significantly, and the system response mainly shows the harmonic and the one sub-harmonic resonance (Figures 4(c) and 4(c′)).

The results of Figures 4 and 5 are further investigated by the time response curve, FFT, phase-plane diagram and Poincaré map. The observations of Figure 6 are as follows: FFT does not indicate any strong peak, phase-plane diagram does not show any specific periods, and Poincaré map shows the fractal structure of strange attractor like Figures 6(d) and 6(d′). From these observations, it is clear that the motion from $\Omega = 0{\cdot}7$ to $1{\cdot}4$ in simulation and from $\Omega = 0{\cdot}81$ to $1{\cdot}26$ in experiment is chaotic (Figure 5). Figure 7 shows period 5, where the FFT shows strong peak at the 1/5 times frequency of the excitation frequency and the phase-plane diagram also shows period 5 with a little mismatch between the experimental result and the simulational result. Period 5 is seen only in the bilinear model free in the clearance. Period 6 is shown in Figure 8 at $\alpha = 0{\cdot}15$. Period 6 appears through a very

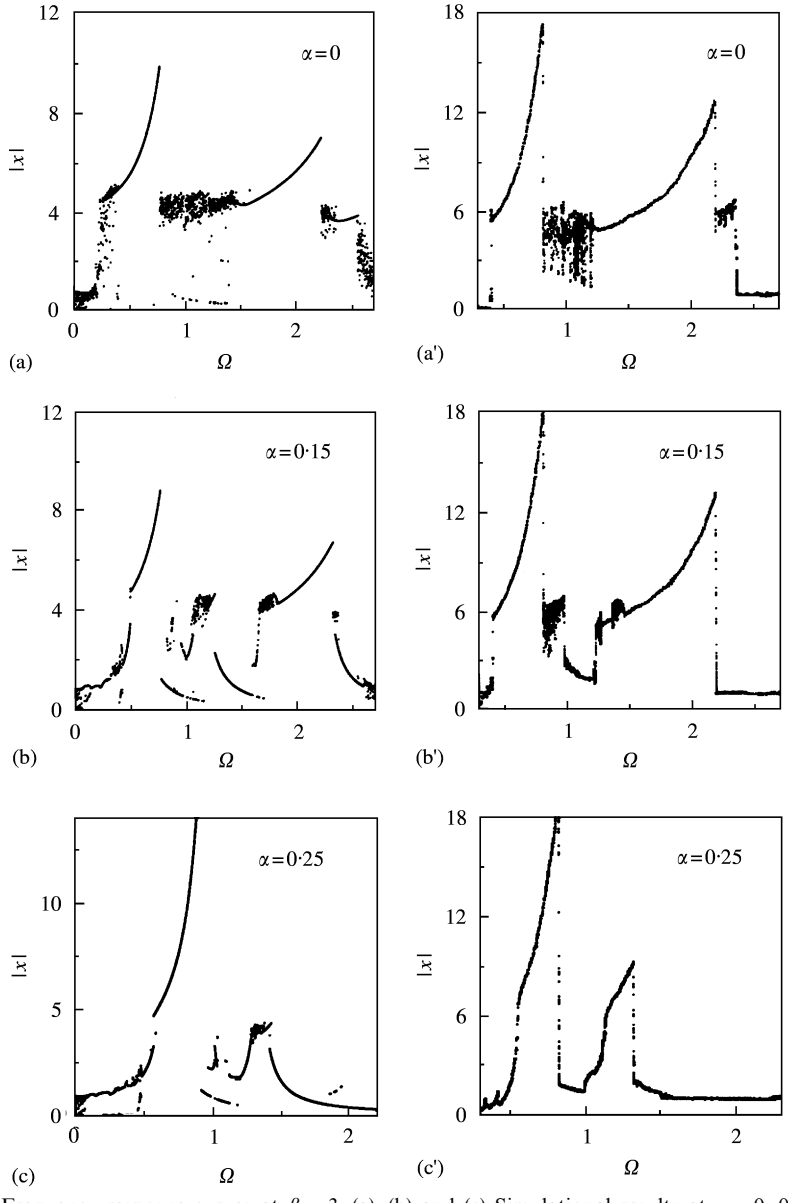

Figure 4. Frequency response curves at $\beta = 3$. (a), (b) and (c) Simulational results at $\alpha = 0$, 0·15 and 0·25

short-frequency region. Poincaré map clearly shows the 6 equilibrium points. FFT shows an interesting result that the higher peak shows at the 1/3 times frequency of the excitation frequency along with the lower peak at 1/6 times frequency of the excitation frequency. Period 3 is shown in Figure 9 at $\Omega = 1{\cdot}85$ in experiment and at $\Omega = 2$ ($f = 0{\cdot}3183$) in simulation.

Figures 10 and 11 show the frequency response curves and the bifurcation diagrams for the values of $\beta = 1$, 2 and 3, while the value of α is kept zero in all of the three cases and other suitable parameters are taken as $\delta_1 = 0{\cdot}1$, $\xi_1 = 0{\cdot}01$, $\xi_2 = 0{\cdot}05$ for the simulation. As the clearance ratio β is increased, more chaos and multiple periods occur, and the extent of

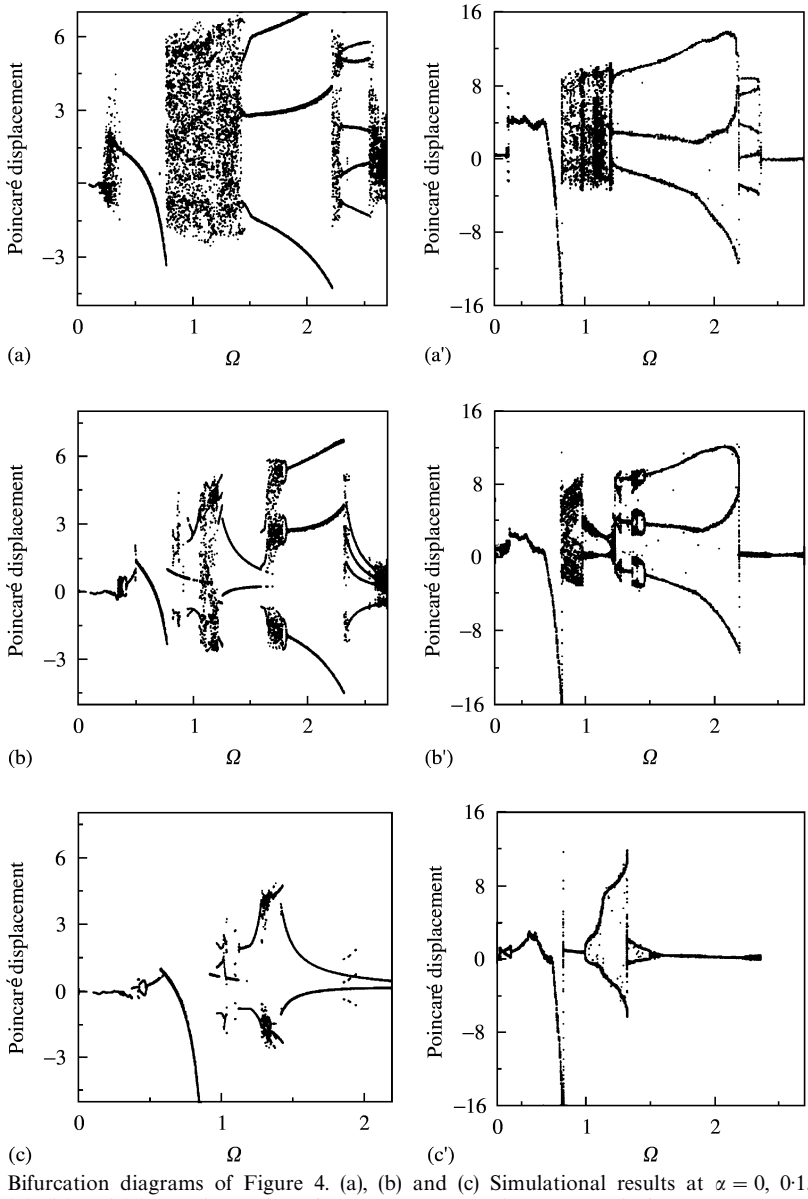

Figure 5. Bifurcation diagrams of Figure 4. (a), (b) and (c) Simulational results at $\alpha = 0$, 0·15 and 0·25 respectively. (a′), (b′) and (c′) experimental results at $\alpha = 0$, 0·15 and 0·25 respectively.

frequency regions of the chaos and the multiple periods is also increased. From the time response, phase plane and FFT analysis (Figures 12 and 13), it is shown that the motion changes at the same frequency from periodic to chaotic or multiple periodic for the bigger values of β.

6. DISCUSSION

Coupling mass and friction forces are not undertaken in the analytical model. The attempt was made to design the experimental set-up as an analytical model. But it was not

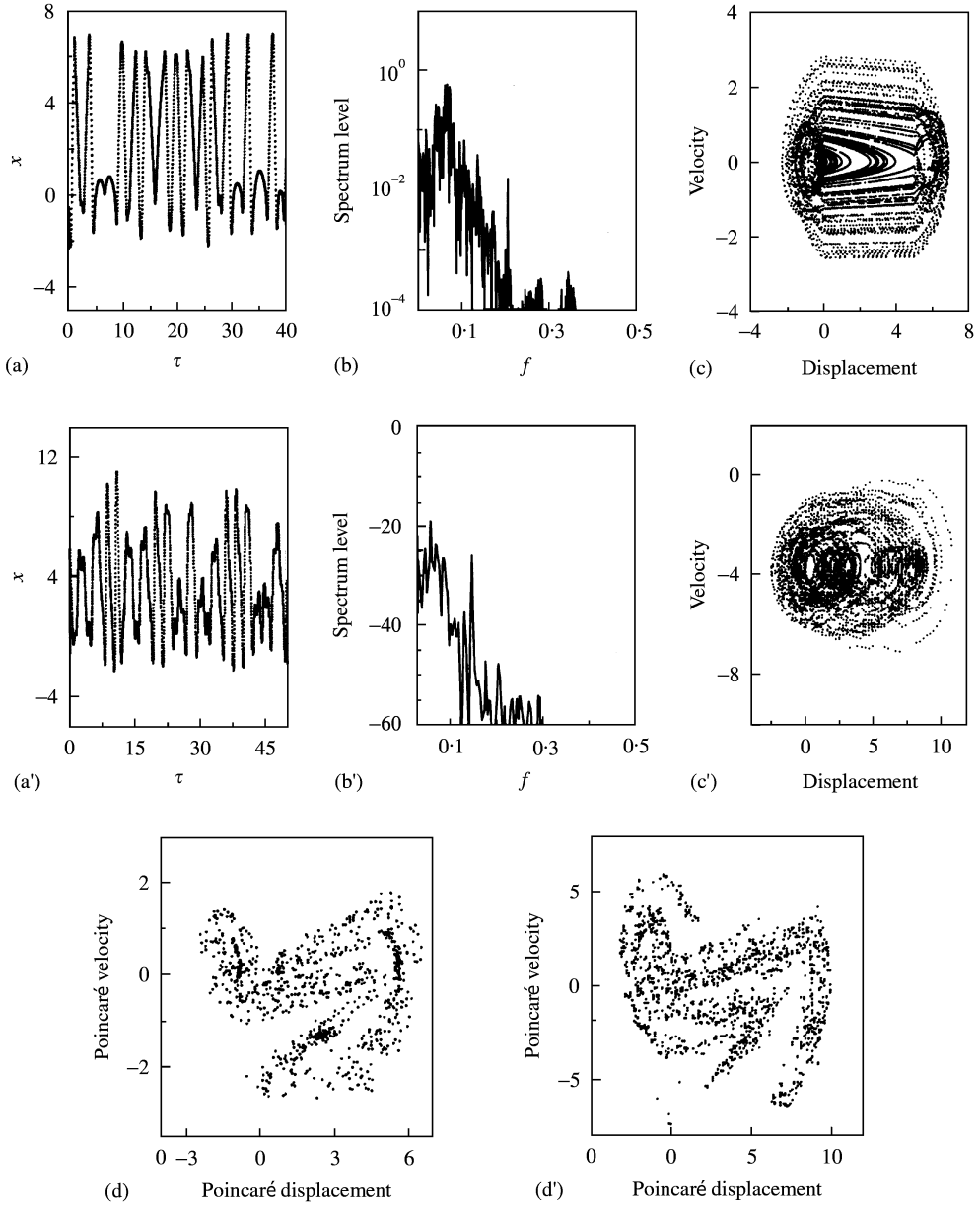

Figure 6. Time response curve, FFT of time response, phase-plane diagram and Poincaré map. (a), (b), (c) and (d) Simulational results at $\Omega = 1{\cdot}3$ ($f = 0{\cdot}2069$) of Figure 4(a). (a′), (b′), (c′) and (d′) experimental results at $\Omega = 0{\cdot}91$ ($f = 0{\cdot}145$) of Figure 4(a′).

possible to avoid coupling mass completely, and a little friction force, especially friction force parallel to spring k_1, is worked against the motion in the experiments. Comparing the system responses of experiment and simulation, these mismatches make some differences in time response, phase plane and also in bifurcation analysis. In spite of these differences, the quality of the motion almost remains the same and significantly comparable to simulation and experiment.

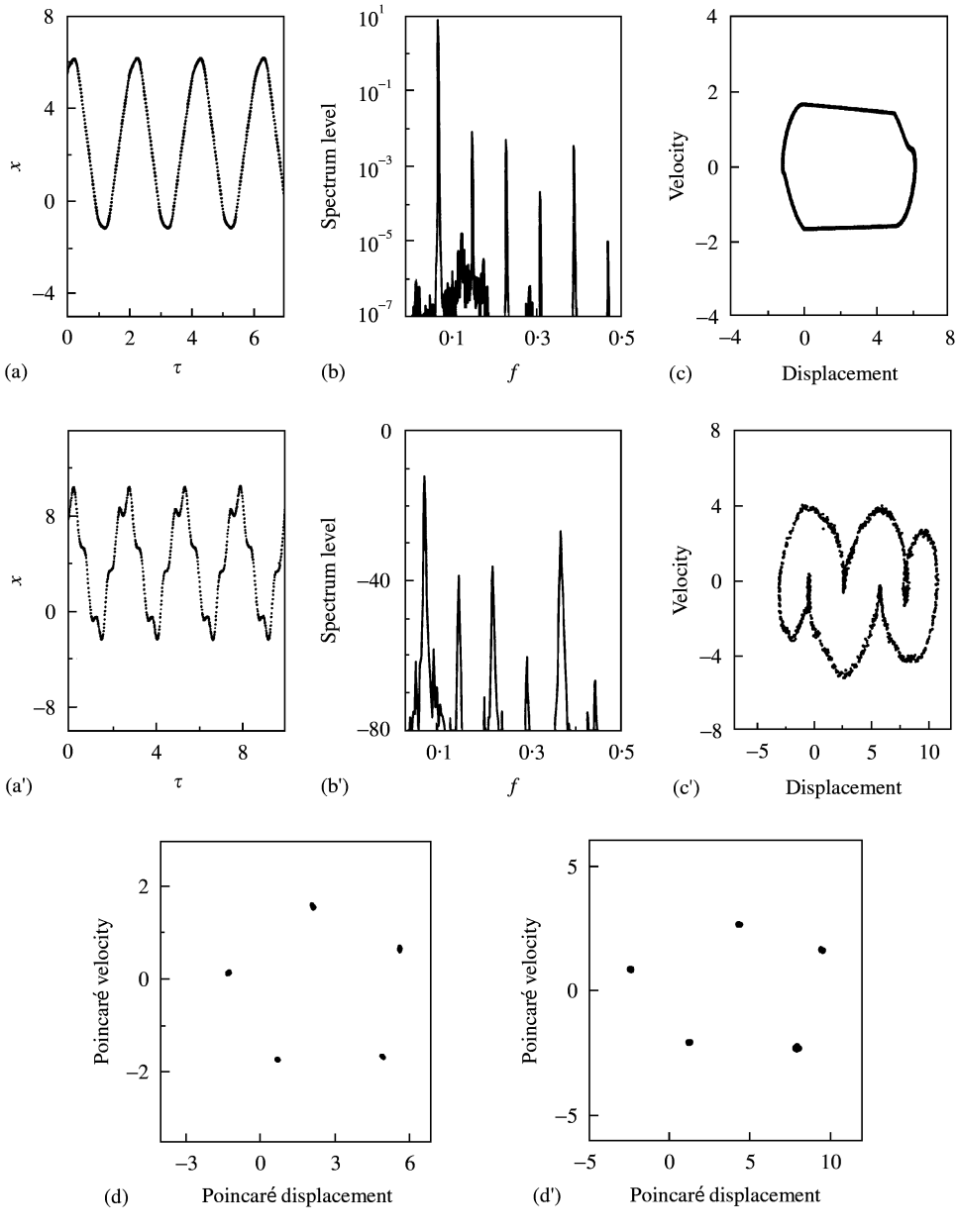

Figure 7. Time response curve, FFT of time response, phase-plane diagram and Poincaré map. (a), (b), (c) and (d) Simulational results at $\Omega = 2{\cdot}45$ ($f = 0{\cdot}3899$) of Figure 4(a). (a′), (b′), (c′) and (d′) experimental results at $\Omega = 2{\cdot}3$ ($f = 0{\cdot}366$) of Figure 4(a′).

The occurring of chaos for the increasing values of β is understandable by the spring characteristic observation (Figure 1(b)). It is assumed that the rightward direction in the spring characteristic model is the positive direction of motion. The motion starts from the balance point and, the position of the balance point is held on the spring k_2. So, the motion starts to travel normally from the spring k_2 to a very low stiffness spring k_1 and then the motion enters into the spring k_2 again for the second time in the positive direction of

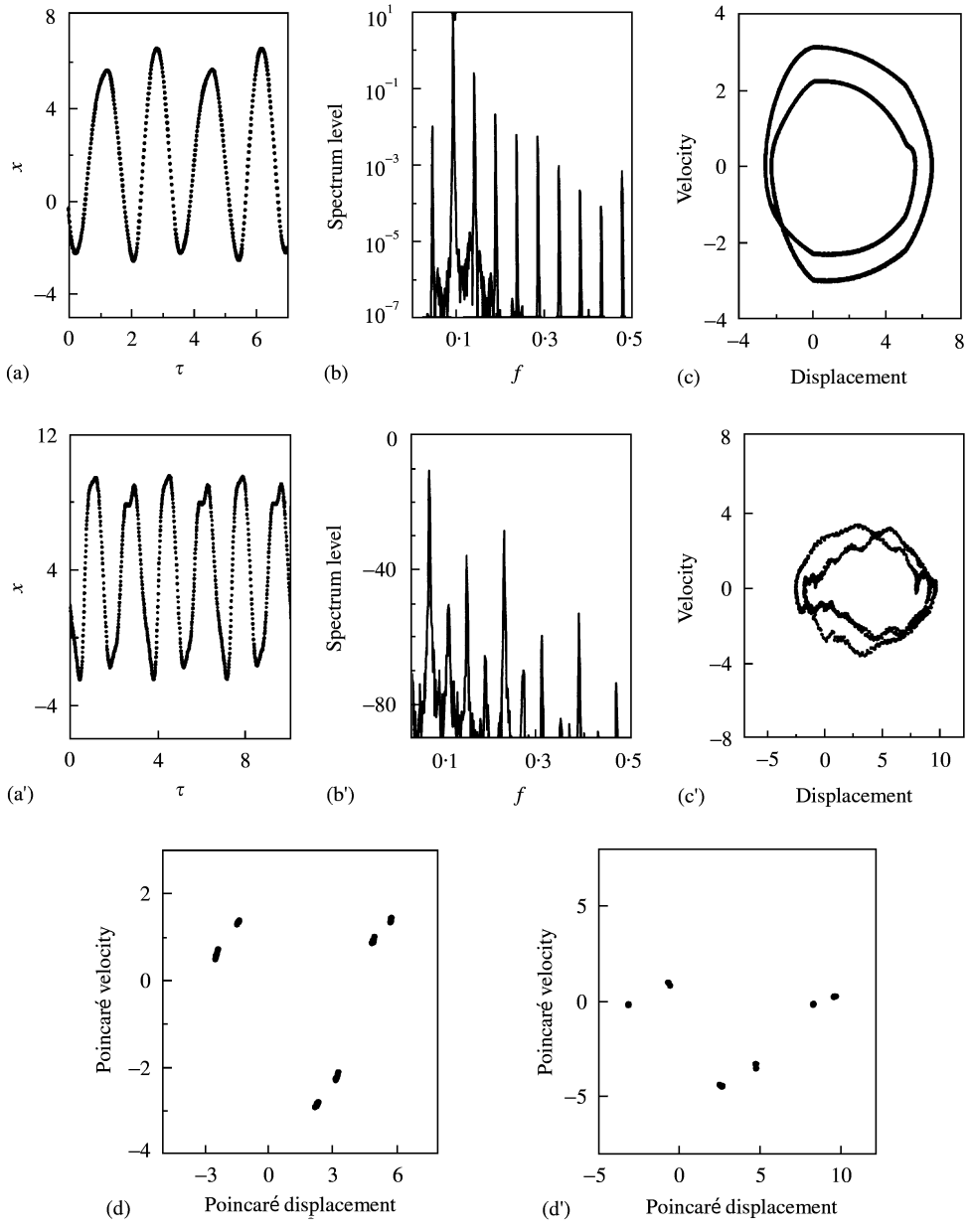

Figure 8. Time response curve, FFT of time response, phase-plane diagram and Poincaré map. (a), (b), (c) and (d) Simulational results at $\Omega = 1{\cdot}8$ ($f = 0{\cdot}2864$) of Figure 4(b). (a′), (b′), (c′) and (d′) experimental results at $\Omega = 1{\cdot}44$ ($f = 0{\cdot}23$) of Figure 4(b′).

motion. The motion returns back through the same path in the negative direction of motion. The velocity changes rapidly at the contact points of the bilinear spring. After suddenly falling down the amplitude at the harmonic resonance, a chaotic phenomenon as an intermittent route to chaos is observed. The motion follows different paths in this chaotic region such as, sometimes the motion returns back from the spring k_1 without entering into the main spring for the second time in the positive direction of motion, sometimes it reaches

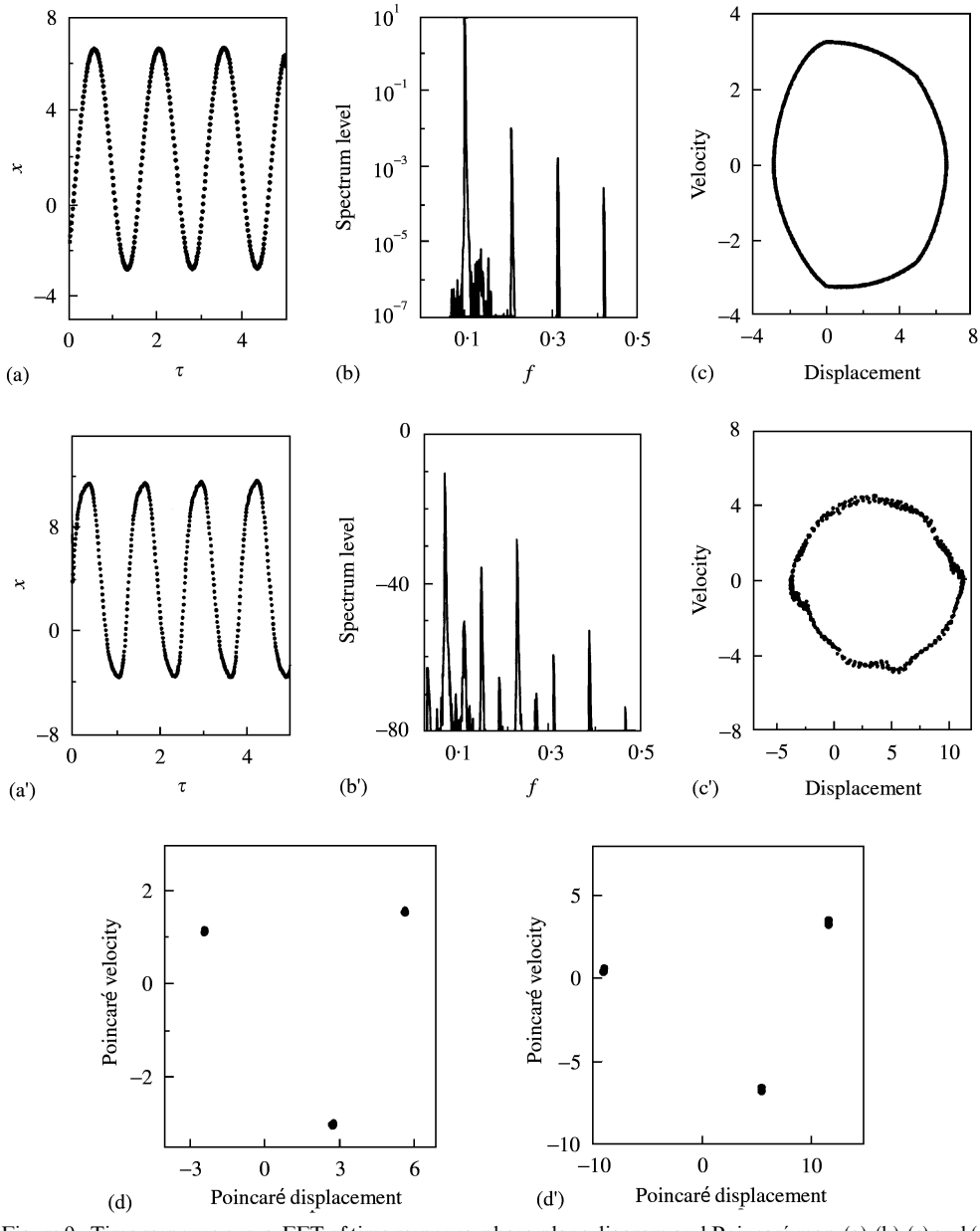

Figure 9. Time response curve, FFT of time response, phase-plane diagram and Poincaré map. (a), (b), (c) and (d) Simulational results at $\Omega = 2$ ($f = 0{\cdot}3183$) of Figure 4(b). (a′), (b′), (c′) and (d′) experimental results at $\Omega = 1{\cdot}85$ ($f = 0{\cdot}295$) of Figure 4(b′).

the main spring for the second time in the positive direction of motion but does not return back up to the balance point in the negative direction of motion, and also sometimes it reaches up to the second contact point and returns back. This observation is also understandable from Figures 6(a) and 6(a′). This motion becomes as periodic to be shown as period 1 or 2, when the motion either travels nearly to the same displacement in the positive and negative directions of motion or travels within the main spring only without entering into the clearance spring.

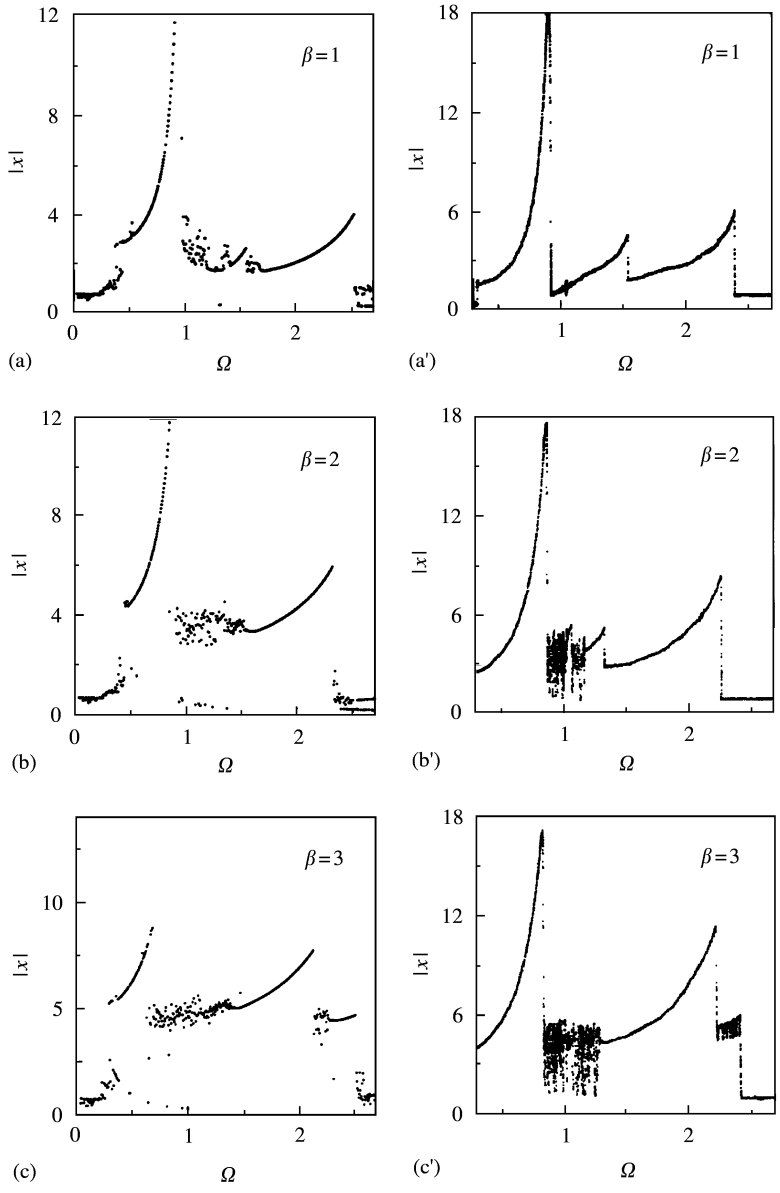

Figure 10. Frequency response curves at $\alpha = 0$. (a), (b) and (c) Simulational results at $\beta = 1, 2$ and 3 respectively. (a′), (b′) and (c′) experimental results at $\beta = 1$, 2 and 3 respectively.

As the spring ratio is decreased with the same clearance ratio, more chaos and multiple periods occur. The fact is that the velocity changes more at the contact points of the spring characteristic model with the small value of the spring ratio. The above discussion prompts one to make another conclusion, that it is easy for the motion to travel to the same displacement in the positive and negative directions of motion for the decreasing of the clearance ratio with the same spring ratio, as the velocity cannot change very rapidly at the contact points.

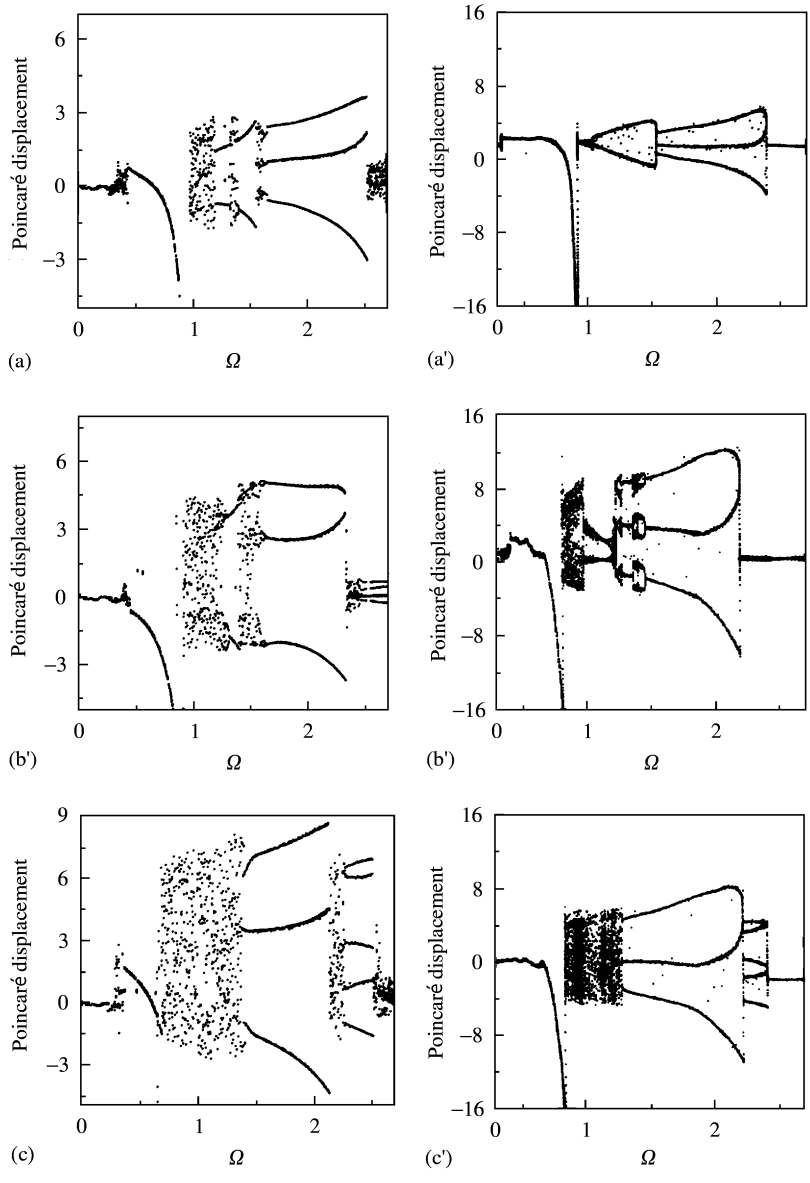

Figure 11. Bifurcation diagrams of Figure 10 at $\alpha = 0$. (a), (b) and (c) Simulational results at $\beta = 1$, 2 and 3 respectively. (a′), (b′) and (c′) experimental results at $\beta = 1$, 2 and 3 respectively.

7. CONCLUSION

The observation of chaos and multiple periods in unsymmetrical bilinear models forms the focus of one balance point model with different values of the spring stiffness ratios and the clearance ratios.

Investigation of the different values of the spring stiffness ratios has revealed that the chaos and the multiple periods are observed more prominently in the bilinear model free in the clearance than that of the model connected by the spring in the clearance. Intermittent

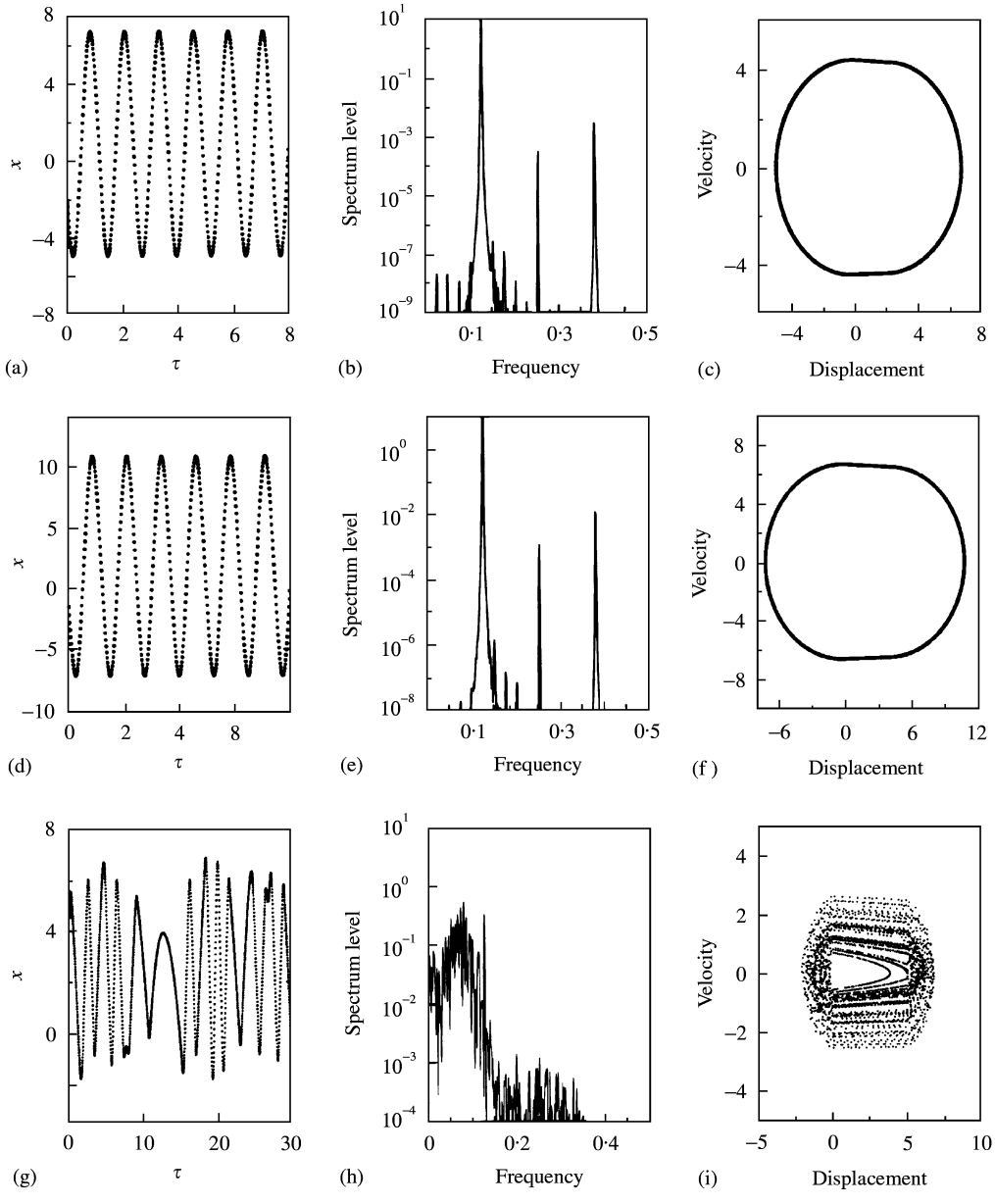

Figure 12. Simulational results at $\Omega = 0{\cdot}8$ ($f = 0{\cdot}1273$) of Figure 10. (a), (b) and (c) Time response curve, FFT of time response and phase-plane diagram, respectively, of Figure 10(a). (d), (e), and (f) Time response curve, FFT of time response and phase-plane diagram, respectively, of Figure 10(b). (g), (h) and (i) Time response curve, FFT of time response and phase plane diagram, respectively, of Figure 10(c).

bifurcation due to the crisis is mainly observed in this observation. Period-doubling bifurcation occurred mainly to the smaller value of the spring stiffness ratio and, further the value of the spring ratio is decreased, the multiple period and the chaotic motions disappeared.

Investigation of the different values of the clearance ratios shows that decreasing of the value of the clearance ratio could attenuate the chaos and the multiple periods.

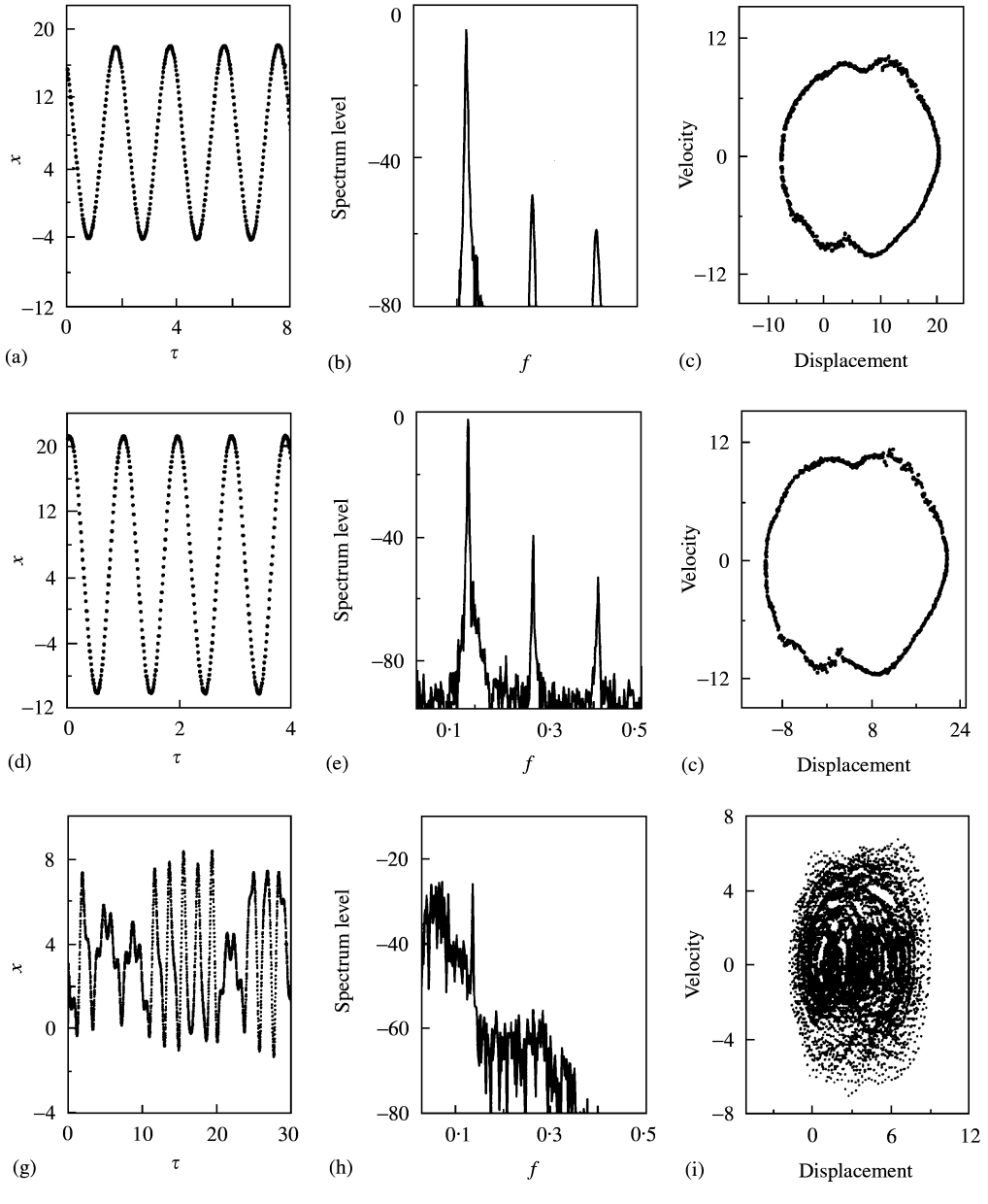

Figure 13. Experimental results at $\Omega = 0{\cdot}85$ ($f = 0{\cdot}136$) of Figure 10. (a), (b) and (c) Time response curve, FFT of time response and phase-plane diagram, respectively, of Figure 10(a′). (d), (e), and (f) Time response curve, FFT of time response and phase-plane diagram, respectively, of Figure 10(b′). (g), (h) and (i) Time response curve, FFT of time response and phase plane diagram, respectively, of Figure 10(c′).

ACKNOWLEDGMENTS

The authors are thankful to Dr. Mitsuhiro Kato, Research assistance of Mie University, for his valuable help to this paper.

REFERENCES

1. S. L. LAU and W. S. ZHANG 1992 *Transactions of the American Society of Mechanical Engineers, Journal of Applied Mechanics* **59**, 153–160. Nonlinear vibrations of piecewise-linear systems by incremental harmonic balance method.
2. S. NATSIAVAS 1990 *International Journal of Non-Linear Mechanics* **25**, 535–554. On the dynamics of oscillators with bi-linear damping and stiffness.
3. K. MIZUTANI and H. MD. ZAHID 1999 *American Society of Mechanical Engineers, Proceedings of the Design Engineering Technical Conferences* (*DETC*99), *CD-Rom, paper Vib*-8297. Clearance and dry friction study in a nonlinear torsional vibration of a rotating machinery.
4. S. DUOBOWSKY and F. FRUEDENSTEIN 1971 *Transactions of the American Society of Mechanical Engineers, Journal of Engineering for Industry* **93**, 305–309. Dynamic analysis of mechanical systems with clearances, Part 1: formation of dynamic model.
5. S. DUOBOWSKY and F. FRUEDENSTEIN 1971 *Transactions of the American Society of Mechanical Engineers, Journal of Engineering for Industry* **93**, 310–316. Dynamic analysis of mechanical systems with clearances, Part II: dynamic response.
6. A. MAHFOUZ and F. BADRAKHAN 1990 *Journal of Sound and Vibration* **143**, 255–288. Chaotic behaviour of some piecewise linear systems, Part I: systems with set-up spring or with unsymmetric elasticity.
7. A. MAHFOUZ and F. BADRAKHAN 1990 *Journal of Sound and Vibration* **143**, 283–328. Chaotic behaviour of some piecewise linear systems, Part II: systems with clearance.
8. R. J. CAMPARIN and R. SINGH 1989 *Journal of Sound and Vibration* **134**, 259–290. Non-linear frequency response characteristics of an impact pair.
9. C. PADMANBHAN and R. SINGH 1995 *Journal of Sound and Vibration* **184**, 767–799. Dynamics of a piecewise non-linear system subject to dual harmonic excitation using parametric continuation.
10. A KHARAMAN and R. SINGH 1990 *Journal of Sound and Vibration* **142**, 49–75. Non-linear dynamics of a spur gear pair.
11. T. E. ROOK and R. SINGH 1994 *Journal of Sound and Vibration* **182**, 303–322. Dynamic analysis of a reverse-idler gear pair with concurrent clearances.
12. C. PADMANBHAN and R. SINGH 1992 *Journal of Sound and Vibration* **155**, 209–230. Special coupling issues in a two-degree of freedom system with clearance non-linearities.
13. Y. B. KIM and S. T. NOAH 1991 *Transactions of American Society of Mechanical Engineers, Journal of Applied Mechanics* **58**, 545–533. Stability and bifurcation analysis of oscillators piece-wise linear characteristics: a general approach.
14. S. NATSIAVAS 1998 *Journal of Sound and Vibration* **217**, 507–522. Stability of piecewise linear oscillators with viscous and dry friction damping.
15. L. B. LIN and A. SEIREG 1994 *Machine Vibration*, vol. 3, 95–106. London: Springer-Verlag. Investigating the multiple steps and chaotic motions of vibrating systems with backlash.
16. S. NARAYANAN and P. SEKAR 1995 *Journal of Sound and Vibration* **184**, 281–298. Periodic and chaotic responses of an sdf system with piecewise linear stiffness subjected to combined harmonic and flow induced excitations.
17. W. WIERCIGROACH, V. W. T. SIN and K. LI 1998 *Chaos, Solitons and Fractals*, vol. 9 (1/2), 209–220. Amsterdam: Elsevier Science Ltd. Measurement of chaotic vibration in a symmetrically piecewise linear oscillator.
18. A. KAHRAMAN and G. W. BLANKENSHIP 1996 *Journal of Sound and Vibration* **194**, 317–336. Interactions between commensurate parametric and forcing excitations in a system with clearance.
19. A. RAGHOTHAMA and S. NARAYANAN 1999 *Journal of Sound and Vibration* **226**, 469–492. Bifurcation and chaos in geared rotor bearing system by incremental harmonic balance method.
20. B. H. TONGE 1986 *Journal of Sound and Vibration* **110**, 69–78. Existence of chaos in a one-degree-of-freedom system.
21. C. GREBOGI, E. OTT and J. A. YORKE 1983 *Physica D* **7**, 181–200. Crises, sudden changes in chaotic attractors and chaotic transients.
22. C. GREBOGI, E. OTT and J. A. YORKE 1982 *Physical Review Letters* **48**, 1507–1510. Chaotic attractors in crisis.
23. F. F. EHRICH 1991 *Transactions of the American Society of Mechanical Engineers, Journal of Vibration and Acoustics* **113**, 50–57. Some observations of chaotic vibration phenomena in high-speed rotor dynamics.
24. Q. FENG and F. PFEIFFER 1998 *Journal of Sound and Vibration* **215**, 439–453. Stochastic model on a rattling system.

25. F. C. MOON 1992 *Chaotic and Fractal Dynamics*, 70–73. New York: John Wiley and Sons, Inc.
26. B. FEENY and F. C. MOON 1994 *Journal of Sound and Vibration* **170**, 303–323. Forced dry-friction oscillator: experiment and numerical modelling.

APPENDIX A: NOMENCLATURE

DIMENSIONAL PARAMETERS

m	mass of the system (kg)
$d_2 - d_1$	extent of clearance (mm)
X_0	harmonic excitation displacement (mm)
X	displacement of mass m (mm)
X_1	displacement of clearance spring (mm)
$k_{i[i=1,2]}$	spring stiffness (N/mm)
$c_{i[i=1,2]}$	damping coefficient (N s/m)
E	amplitude of harmonic excitation (mm)
ω	harmonic excitation speed (rad/s)
$p_{i[i=1,2]}$	$\sqrt{k_{i[i=1,2]}/m}$

NON-DIMENSIONAL PARAMETERS

τ	$p_2 t$
δ_1	d_1/E
δ_2	d_2/E
Ω	ω/p_2
$\xi_{i[i=1,2]}$	$c_{i[i=1,2]}/mp_2$
α	spring ratio (clearance spring stiffness/main spring stiffness) $= k_1/k_2$
β	clearance ratio (clearance gap/amplitude of harmonic excitation) $= (d_2 - d_1)/2E$)
f	$\Omega/2\pi$